REPORT DOCUMENTATION PAGE

Form Approved
OMB No. 0704-0188

1. REPORT DATE *(DD-MM-YYYY)*	2. REPORT TYPE	3. DATES COVERED *(From - To)*
30-05-2006	Final Report	01 Aug 05 - 30 Apr 06

4. TITLE AND SUBTITLE
Throughput Optimization Via Adaptive MIMO Communications

5a. CONTRACT NUMBER
FA9550-05-C-0103

5b. GRANT NUMBER

5c. PROGRAM ELEMENT NUMBER

6. AUTHOR(S)
Zhu, Weijun
Daneshrad, Babak

5d. PROJECT NUMBER

5e. TASK NUMBER

5f. WORK UNIT NUMBER

7. PERFORMING ORGANIZATION NAME(S) AND ADDRESS(ES)
Silvus Communication Systems, Inc.
11835 W. Olympic Blvd, Suite 745
Los Angeles, CA 90064

8. PERFORMING ORGANIZATION REPORT NUMBER

9. SPONSORING/MONITORING AGENCY NAME(S) AND ADDRESS(ES)
Air Force Office of Scientific Research/NM (Dr. Jon A. Sjogren)
875 North Randolph Street
Suite 325, Room 3112
Arlington, VA 22203

AFRL-SR-AR-TR-06-0335

12. DISTRIBUTION/AVAILABILITY STATEMENT
Distribution A:
Approved for public release, distribution unlimited

13. SUPPLEMENTARY NOTES

14. ABSTRACT

A MIMO-OFDM system for aircraft to urban ground non-line-of sight communications that supports programmable bandwidth efficiency between 0.25 bps/Hz and 20 bps/Hz has been designed. The system supports the whole range of MIMO techniques, namely spatial multiplexing, beamforming, space-time coding, and diversity processing. The system is, on a packet by packet basis, configurable in terms of number of antennas, MIMO techniques, modulation order, channel coding type, channel coding rate, channel training length, and channel tracking overhead. The feasibility and performance has been verified in the developed Matlab end-to-end simulation system and on the Silvus DSP MIMO Testbed.

15. SUBJECT TERMS
MIMO, OFDM, Non-Line-of-Sight, Doppler, Adaptive Communications

16. SECURITY CLASSIFICATION OF:			17. LIMITATION OF ABSTRACT	18. NUMBER OF PAGES	19a. NAME OF RESPONSIBLE PERSON
a. REPORT	b. ABSTRACT	c. THIS PAGE			Weijun Zhu
Unclassified	Unclassified	Unclassified	UU	27	19b. TELEPHONE NUMBER *(Include area code)* (310) 694-3597

Throughput Optimization Via Adaptive MIMO Communications

Final Report May 30th, 2006

Air Force Office of Scientific Research (AFOSR)

Contract No. FA9550-05-C-0103

STTR Topic No. AF05-T022

Seamless Non-Line-Of-Sight Communications for Urban Warfare

Name of Contractor: **Silvus Communication Systems, Inc.**
Project Scientist: **Weijun Zhu**
Business Address:
11835 W. Olympic Blvd. #745
LA, CA 90064
Phone Number: **(310) 694-3597**

Effective Date: **August 1, 2005**
Short Title of Work: **Throughput Optimization via Adaptive MIMO Communications**
Contract Expiration Date: **May 30, 2006**
Reporting Period: **08/01/05 – 04/30/06**

Disclaimer

UNCLASSIFIED

1. Introduction

This final report presents all work that the Silvus-UCLA team have conducted on AFOSR STTR Contract FA9950-05-C-0103, TITLE: Throughput Optimization via Adaptive MIMO communications. This report includes and supersedes all previous quarterly progress reports and includes the work completed in the last performance period from April 1st 2006 to May 31st 2006. The work performed is divided into the following five categories, each of which will be reported in a separate section.

- End-to-end matlab packet simulation platform.
- Low density parity check code (LDPCC).
- Field trials with Silvus DSP MIMO testbed.
- High mobility extension.
- Preparation for FPGA real-time implementation.

To be self contained, the report starts with a brief problem statement and our approach.

Identification and Significance of the Problem

Since the early work of Foschini and Gans [6][7] and Teletar [11] on the capacity of multiple antenna radio (MAR), a great body of work has shown the potential for MIMO based communications to deliver unprecedented spectral efficiency in multi-path rich environments. To a large extent these studies have been theoretical and simulation based [12] [13]. A few experimental MIMO systems have also been reported in the literature, including some from the members of the Silvus team [14][8][9]. However, these trials have been mostly limited to controlled environments, mostly indoors, but a few outdoor mobile environments as well.

The application of MIMO communications to the needs of UAV based communications is not fully understood. Indeed a UAV borne MIMO link poses several unique challenges both from an algorithmic/protocol point of view, as well as a hardware architecture point of view. For a UAV based system operating in dense urban environments, whether below or above the building clutter, the following unique challenges exist:

- A highly dynamic channel due to the high mobility of the UAV,
- A channel whose capacity and degrees of freedom will vary significantly with UAV altitude,
- A diversity of mission requirements including
    - Use in reconnaissance missions behind enemy lines (10s of Kbps)
    - Use as a stove-pipe relay node (a few Mbps)
    - Use as an element of a backbone node (100s of Mbps),
- A diversity of the UAV platforms in use by the Air Force,
- A potential deployment in a mobile ad-hoc network (MANET).

The high mobility and changing characteristics of the UAV channel with altitude imply that the radio system must be adaptive in time and adaptive in space to exploit these characteristics. The diversity of mission requirements implies that the radio must adapt the bandwidth, the spectral efficiency, and the carrier frequency to be successful in all scenarios. In addition, the ability to be used in a variety of UAV

platforms and to easily integrate into a mobile ad-hoc network (MANET) environment mandates a radio system that is both hardware and protocol adaptive.

The work will culminate in a complete system level design as well as a scalable hardware architecture that will allow the proposed MIMO system to scale with the capabilities of the UAV and the mission requirements.

2. Approach

This section outlines our general approach to addressing the needs of the UAV based MIMO communications system.

High throughput communications will be addressed by realizing that MIMO techniques, although quite powerful, are only an element of an overall physical layer solution. MIMO must be designed to operate in-harmony and in complementary fashion with the other physical layer parameters. As such achieving the highest possible throughput in a given environmental conditions will be achieved by the proper choice of:

- MIMO processing (spatial multiplexing, or space-time coding, or diversity processing, or smart antenna processing)
- FEC code and rate
- Constellation size and type of modulation
- Signal bandwidth
- Carrier frequency

Our system implements all four variants of multi antenna techniques (spatial multiplexing, space-time coding, diversity processing, and smart antenna processing). In an attempt to get as close to the Shannon capacity as possible we incorporate advanced LDPC (low density parity check) codes. Realizing that the power of LDPC codes come at the price of decoder complexity, we also incorporate bit interleaved convolutional codes into our system requirements so as to enable us to operate with low decoder complexity over good channels. To combat multipath and to ensure high spectral utilization we have adopted an OFDM based signaling scheme. Over the past several years OFDM has become the modulation of choice for both wireline and wireless communication systems, as it has been adopted for DVB standards, wireless LAN, and other standards.

Diversity of mission requirements dictate a high degree of adaptability in the physical layer and radio architecture itself. Moreover, the widely varying conditions of the wireless channel call for a great degree of configurability and robustness from the radio unit. Our approach to addressing the diversity of mission requirements is to incorporate a great deal of adaptability into the radio system. This includes adaptability in the modulation format, coding rate, bandwidth carrier frequency, and MIMO processing. Underlying the adaptability of the signal bandwidth, and center frequency is a highly agile radio architecture that we will be explored as part of the proposed work.

High Doppler Communications refers to the case where the rate of change of the channel is high. In general the Doppler frequency, f_d, is defined as v/λ (λ is the wavelength of the carrier and v is the relative speed between the transmitter and receiver), represents the speed at which the channel changes. We overcome the limitations of extreme mobility through pilot symbol assisted modulation technique.

Radio form factor sufficiently small to fit into UAV payload. Although the issue of the final size of the radio is not directly addressed as part of the phase 1 effort, it is nonetheless an important issue that must be kept in mind in developing the system. As part of the phase one effort we searched for available processing and RF platforms with an eye towards being able to fit them into the belly of a small UAV. The processing capability of such platforms might dictate, in phase II, the specific MIMO configurations that might be supported.

Over the course of the one year period of this project, the Silvus and UCLA team have successfully completed the following tasks:

- Matlab MIMO-OFDM Simulation System.
- Design and simulation of Low Density Parity Check Code.
- Verification with Silvus DSP MIMO Testbed.
- Design and Simulation for High Mobility Extension.
- Preparation for Real-Time Implementation on FPGA.

Each item will be reported in a separate section hereafter.

3. Matlab MIMO-OFDM Simulation System

A packet structure has been developed to support realistic end-to-end physical layer packet simulation. The developed packet structure is highly portable and support interoperability with both SISO and MIMO enabled nodes. Moreover given the size and power constraints of a UAV based communication system, there might be times when the desired QoS can be met in an energy efficient SISO mode. The packet structure does not preclude this. Additionally, we strive to develop the packet structure in such a way as to minimize overhead, effectively increasing goodput as compared to over the air data rate. Figure 1 shows the top-level packet structure. It consists of a universal SISO header that is understandable by all systems. The Mode identifier indicates the particular MIMO configuration that is used for the remainder of the packet, and the receiver dynamically switches to the proper decoder for the given mode.

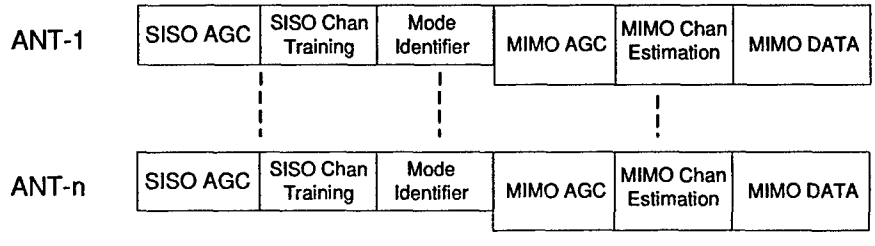

Figure 1. Physical Layer Frame Structure

The packet mainly consists of six fields. The first three components only require one transmit and one receive antennas to work.

1. SISO AGC (Automatic Gain Control) Preamble. The SISO AGC field is intended to assist the receiver for packet detection, gain control, and optionally coarse frequency and symbol timing synchronization.
2. SISO Channel Training. The SISO Channel Training field is intended to assist the receiver for symbol timing, carrier frequency synchronization, and channel estimation.
3. Mode Identifier. The Mode Identifier tells the receiver the format of the packet following this field. Table 1 lists all the supported modes that can be selected in the Mode Identifier. The Mode Identifier is protected with CRC to prevent the receiver decoding based on wrong assumptions.

Table 1. Supported Modes of The Packet Structure

Mode Description	Supported Values
Number TX Antennas	1, 2, 3, 4
Number of Multiplexed Spatial Streams	1, 2, 3, 4
Space Time Block Code	Yes or No
Constellation	BPSK, QPSK, 16QAM, 64QAM
Channel Coding	Binary Convolution Code or LDPC
Packet Length	0 ~ 2^{16}-1, bytes
Coding Rate	1/2, 2/3, 3/4, 5/6
MIMO Channel Training Length	0 ~ 4, symbols
High Mobility Support Extension	Yes or No
Transmit Beamforming	Yes or No

4. MIMO AGC Field. The MIMO AGC Field assists the receiver to adjust receiver gain settings for the MIMO section of the packet. This field is not transmitted for SISO mode.
5. MIMO Channel Training Field. The MIMO Channel Training Field assists the receiver for MIMO Channel estimation and possibly improvement of carrier and timing synchronization. This field is not transmitted for SISO mode.
6. Data Field. The Data field contains both payload and pilots. Two different pilot schemes are supported for best tradeoff between bandwidth efficiency and support for mobility. In the scenario of low mobility, low order constellation, or short packet length, a few sub carriers are dedicated to transmit pilots to assist the receiver for tracking phases and frequency offset. When the channel changes significantly during the packet, a more sophisticated pilot scheme is used. In this scheme, pilot symbols are spread across the frequency-time domain. The receiver could use these pilot symbols to estimate and track channel continuously. For detailed information on the pilot scheme for high mobility, refer to Section **Error! Reference source not found.**.

Using the packet structure described above, a complete simulation system has been efficiently implemented in Matlab. Certain functions are implemented in Mex functions using C/C++ to achieve good simulation speed. The implementation is highly modularized and parameterized for easy upgrade as the requirements evolve as well as for providing a simulation environment to test innovative ideas. The system is a complete packet level end-to-end simulation system, including packet generation, all major hardware/RF impairments, sophisticated MIMO channel model, and complete reference receiver. Figure 2 and Figure 3 show the block diagram of the transmitter and the receiver.

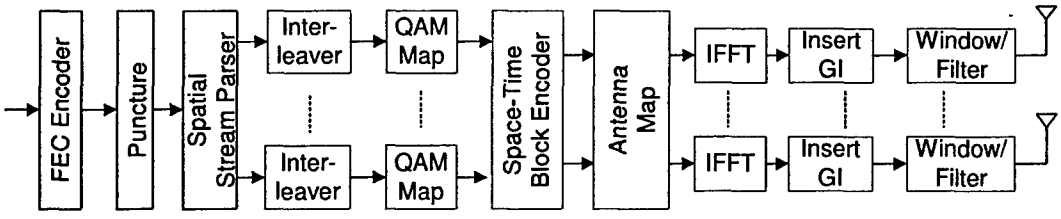

Figure 2. Functional Block Diagram of the Transmitter

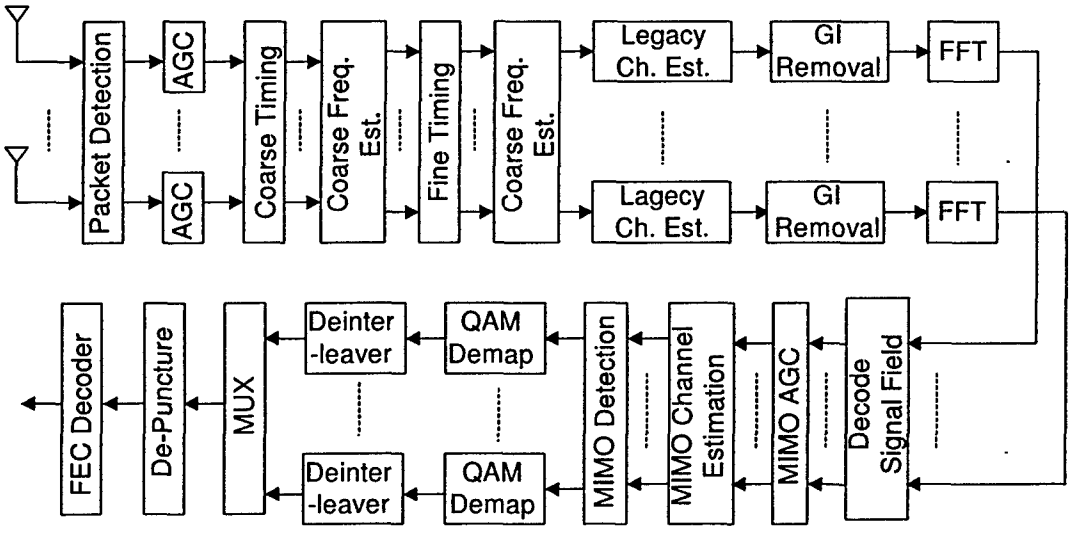

Figure 3. Functional Block Diagram of the Receiver

The simulation system supports the following features:

- Any combination of antenna configuration, up to 4 transmit antennas and 4 receive antennas.
- Spatial multiplexing with up to 4 spatial streams.

- Space-time block codes.
- Spatial cyclic delay diversity.
- Hybrid space-time and spatial multiplexing system.
- Binary convolutional code and LDPCC with variable coding rate, 1/2, 2/3, 3/4 5/6.
- Transmit per-subcarrier beamforming.
- Space-frequency-time 3 dimensional interleaver for maximum coding diversity gain.
- Different constellation size: BPSK, QPSK, 16QAM, 64QAM.
- Soft/hard decision Viterbi decoder.
- Layered fast LDPCC decoder.
- Versatile channel model with programmable delay and power profile and Doppler spread.
- Programmable hardware and RF impairments such as carrier frequency offset, phase noise, power amplifier non-linearity, and I/Q imbalance.
- Fixed point model for key components such as MIMO detection and synchronization.

All these features can be easily controlled by toggling flags and/or setting parameters. For instance, most part of the receiver could be instructed to use perfect information to assess the implementation loss on an individual module basis. The simulation system also features a complete low-complexity high performance Silvus proprietary receiver that can serve as a design for real-time implementation. The simulation platform that the Silvus-UCLA team developed has become a valuable tool for trying out innovative ideas. The rest of the section presents some of the results obtained using this simulation platform.

Simulation results

The results presented here are the results of full system simulations in various channel scenarios. It is a complete physical layer end to end packet simulation which includes all the necessary transmitter and receiver algorithms. Major hardware impairments are also included. All algorithms are practical in terms of hardware implementation. In fact, if a real-time implementation is required, all those algorithms can be directly translated into fixed point implementation and mapped onto hardware.

The following is a list of important parameters of the simulations that were reported here.

- 4 transmit antennas with 4 spatial data streams
- 4 receive antennas
- 20MHz bandwidth
- 2.4GHz carrier frequency
- Sub-carrier spacing 312.5KHz
- 56 effective carriers, 52 data carriers + 4 pilot carriers
- Bit interleaved coded modulation with binary convolution code and QPSK, 16QAM, 64QAM
- Jakes model[21] is used for simulating time varying fading
- Frequency selective multi-path fading model is based on temporal multi-clustering model proposed in [22]. It has an exponential delay and power profile

The following hardware impairments were introduced in the simulation.

- Phase noise on both TX and RX sides. The phase noise model for the IEEE next generation wireless LAN standard is used. It represents a phase noise model one would observe in a typical inexpensive commercial grade system. Refer to [19] for the details of this model.
- Nonlinearity of power amplifiers. The model for the IEEE 802.11b is used. An output power backoff 10dB is used in the simulation. Refer to [20] for details.
- Carrier frequency offset. A frequency offset of 130 KHz is used for all simulations.

The following list describes the important features of the receiver algorithm.

- A two-stage packet detection and OFDM symbol timing algorithms are used. First stage algorithm keeps searching for the SISO AGC preamble in the incoming signal. It has a very low complexity. Once it finds the preamble, a packet is declared to be found. The second stage uses the SISO Channel Training field to fine tune OFDM symbol timing. Carrier frequency estimation, noise variance estimation, and SISO channel estimation are done at the same stage.
- MIMO Channel estimation is done once using the MIMO Channel training field. There is no channel tracking afterwards. See Section **Error! Reference source not found.** for our simulation results with channel tracking.
- MIMO Detection is based on the principle of linear minimum mean square error (LMMSE) detection.
- A fast QAM soft demapper with complexity linear to the number of bits is developed and used in the simulation.
- Phase noise tracking is performed on a symbol by symbol basis using the embedded pilot carriers.
- A soft input sliding window Viterbi algorithm is used to decode convolution code.

The simulations aim to examine the performance of the whole system from three different perspectives.

- Performance as a function of Doppler spread for QPSK, 16QAM, and 64QAM at a speed of 5MPH, 100MPH, and 500MPH. 500MPH is not simulated for 16QAM and 64QAM as the performance is not acceptable even with ideal synchronization and no RF impairments (See Figure 5 and Figure 7). A flat fading channel is chosen in this case.
- Performance as a function of delay spread at a RMS delay spread of 0ns, 15ns, 50ns, and 150ns. 16QAM and 5MPH is used for this simulation.
- Performance as a function of packet length for QPSK. The speed is set to 100MPH

The results are summarized in the following plots and paragraphs. As a comparison, part of the results for ideal synchronization and no RF impairments are also included.

Performance vs. Speed

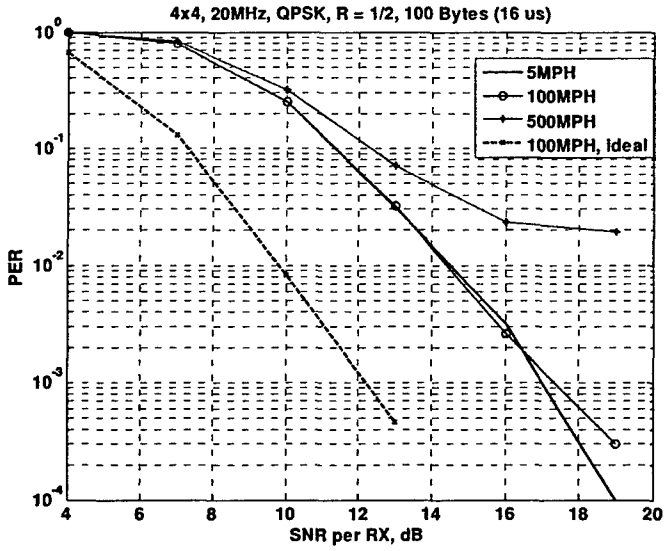

Figure 4. Packet Error Rate for QPSK at Different Speed

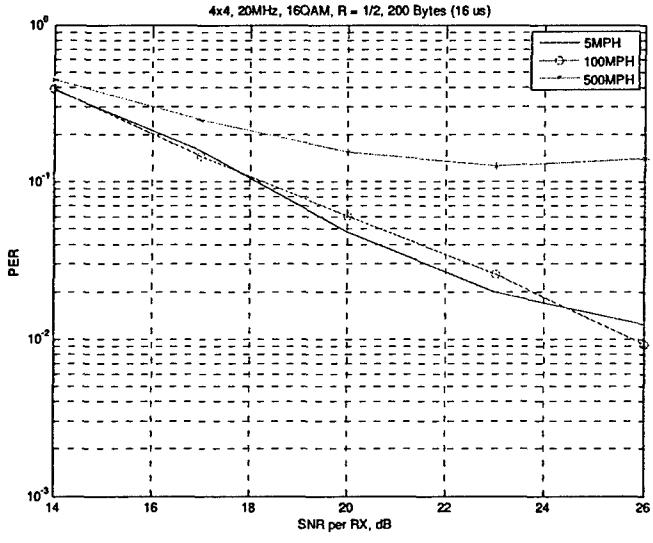

Figure 5. Performance 16QAM with Ideal Synchronization and No Hardware Impairments

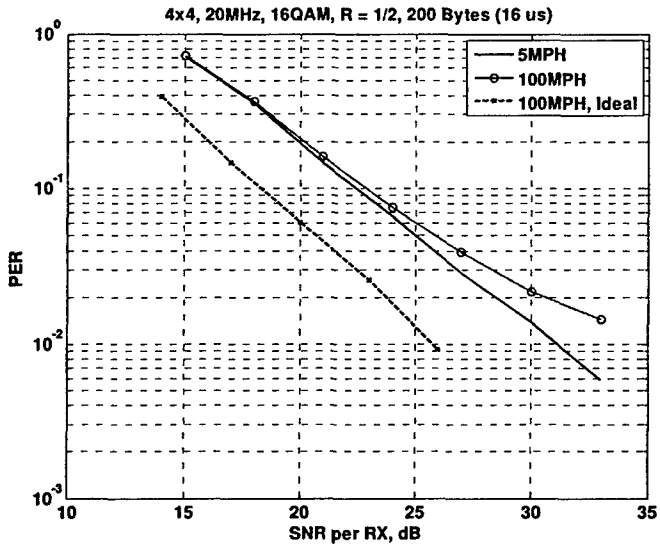

Figure 6. Packet Error Rate for 16QAM at Different Speed

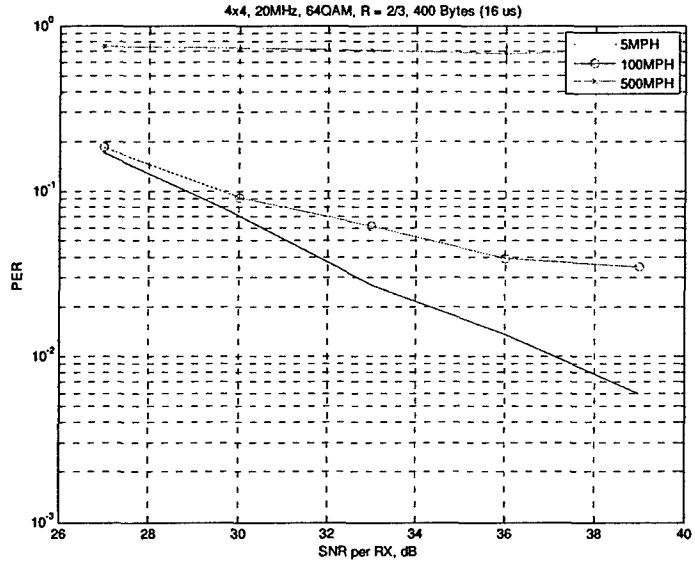

Figure 7. Performance of 64QAM with Ideal Synchronization and No Hardware Impairments

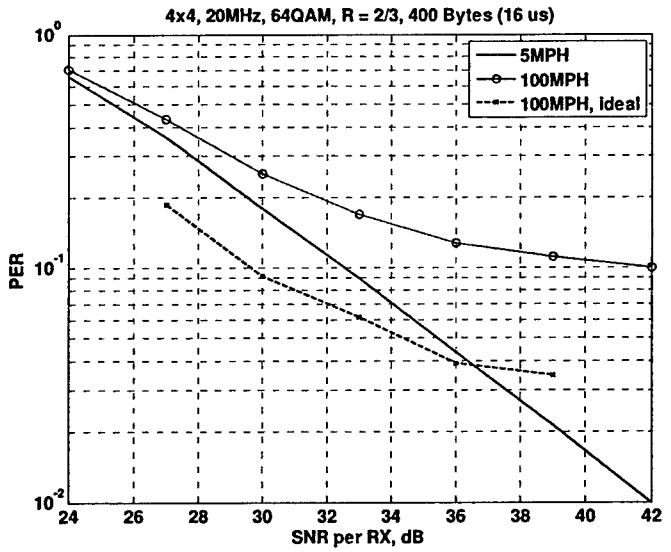

Figure 8. Packet Error Rate for 64QAM at Different Speed

Figure 4, **Figure 6**, and **Figure 8** show the performance vs. speed simulation results. These results show that if the required packet error rate is 10% with 100-Byte long packets, QPSK is applicable at a speed more than 500MPH, 16QAM is applicable at a speed more than 100MPH, and 64QAM requires 42dB SNR at a speed of 100MPH. The RF impairments and practical synchronization algorithm introduces an approximate loss of 4dB, 5dB, and 12dB at 10% PER and 100MPH, for QPSK, 16QAM, 64QAM respectively. It is clear that if high constellation such as 64QAM is desired at high speed, the receiver needs to perform channel tracking to combat the time-varying fading.

Performance vs. Delay Spread

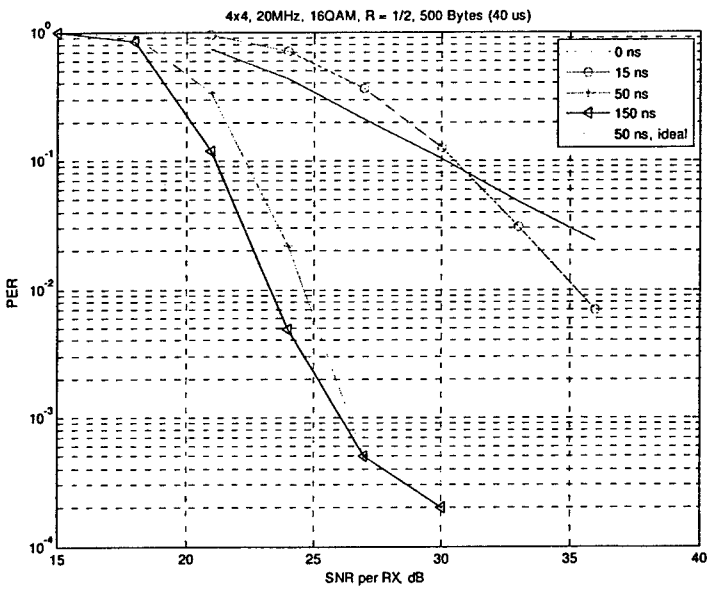

Figure 9. Packet Error Rate for 16QAM with Different Delay Spread

Figure 9 shows the performance of the system using 16QAM with practical receiver and RF impairments. Interestingly, the diversity effect that 15 ns delay spread offers does not exhibit itself for low PER. However, a larger delay spread such as 50ns or 150ns offers significant advantage over flat fading. For instance, 50 ns delay spread offers about 7dB gain at 10% PER compared to flat fading. The synchronization and RF impairments introduces about 4dB loss.

Performance vs. Packet Length

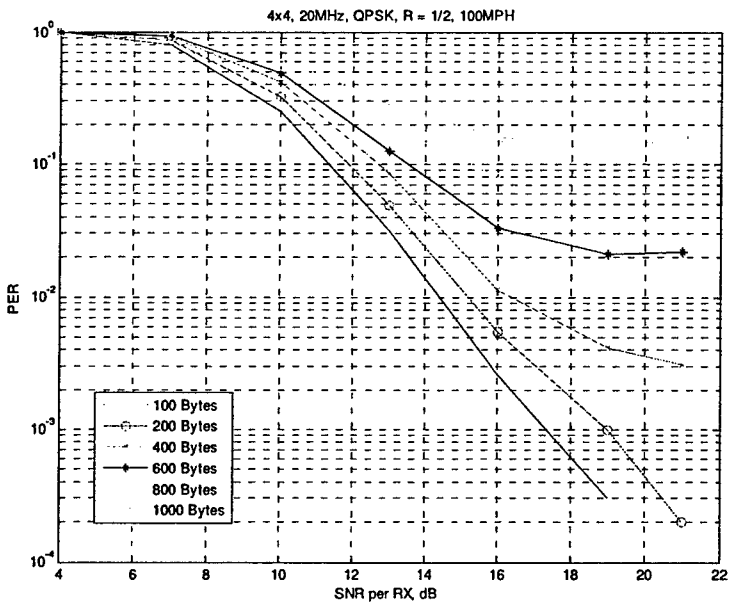

Figure 10. Packet Error Rate of QPSK with Different Packet Size

Figure 10 shows that if 10% is the target packet error rate, 800 bytes is the maximum packet size the simulated system supports. A significant error floor is observed when the packet length is above 400 bytes.

Conclusion Drawn from the Simulation Results

With QPSK, the current MIMO-OFDM system works reasonably well at a speed less than 100MPH. For short packet communication, even higher constellation such as 16QAM and 64QAM or higher speed such as 500MPH is possible. If more bandwidth efficiency and/or higher speed are desired, a channel tracking algorithm designed for time varying channel is required. This work will be reported in Section **Error! Reference source not found.**.

4. Design and Simulation of Low Density Parity Check Code

Low density parity check codes are linear binary block codes with parity check matrices containing mostly zeros and only small number of ones. LDPC codes can be described by an *MxN* parity check matrix, H, or via a graphical representation called bipartite graph. *M* rows of parity check matrix specify each of the *M* constraints on codeword bits and *N* columns define the codeword length. Similarly,

bipartite graph contains N *bit nodes*, one for each bit (column of H) and M *check nodes*, one for each of the parity checks (row of H). Figure 11 illustrates the parity check matrix, H, for a simple (7, 3) code and corresponding bipartite graph, which provides a graphical representation of the parity check matrix and assists in the understanding of the iterative soft decoding algorithm. In the Bipartite graph (Figure 11) of a (7, 3) code, *bit nodes* are denoted using circles and *check nodes* are denoted using squares. The *check nodes* are connected to *bit nodes* they check or in other words *check node j* is connected to a *bit node i* whenever element h_{ji} in H is a 1.

$$H = \begin{array}{c} \begin{matrix} v0 & v1 & v2 & v3 & v4 & v5 & v6 \end{matrix} \\ \begin{bmatrix} 1 & 1 & 1 & 1 & 0 & 0 & 0 \\ 1 & 0 & 0 & 0 & 1 & 1 & 0 \\ 1 & 1 & 0 & 1 & 0 & 0 & 0 \\ 0 & 0 & 0 & 0 & 1 & 1 & 1 \end{bmatrix} \end{array} \begin{matrix} c0 \\ c1 \\ c2 \\ c3 \end{matrix}$$

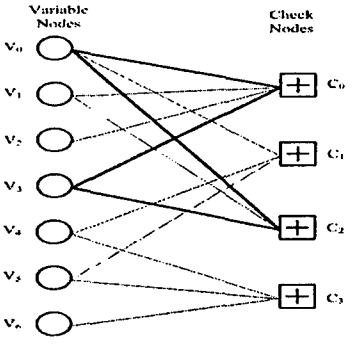

Figure 11, Bipartite graph of a (7,3) code

In the following, three variations of the LDPC decoding algorithm, namely sum-product, Offset Min-Sum, and Layered Decoding algorithms are discussed and corresponding simulation results are presented.

Sum Product Algorithm

The sum-product decoding algorithm (SPA) [23][24] works iteratively by passing messages on the edges of the associated bipartite graph. The messages are the Log-Likelihood Ratios (LLRs), where the sign of the message represent the binary digit and the magnitude denotes the reliability of the message.

Before describing the sum-product algorithm, the notation is introduced. The set $V(j)=\{i: H_{j,i}=1\}$ defines the bit nodes that are connected to check j and the set of check nodes that are connected to bit i is denoted as $\mu(i)=\{j: H_{j,i}=1\}$. A set $V(j)$ with bit i excluded is referred by $V(j)\backslash i$ and a set $\mu(i)$ with check j excluded is denoted by $\mu(i)\backslash j$. $Q_{i,j}$ defines a message sent from bit node i to check node j and $R_{j,i}$ refer to the message that is passed from check node j to bit node i. The sum-product algorithm starts with an initialization step and then iterations continue by exchanging messages between bit and check nodes. Decoding is stopped when all the parities are satisfied or a maximum number of iterations are reached. The main steps of the decoding are summarized as follows.

1st Step: Initialization: Each bit node is assigned a posteriori log-likelihood ratio, $L_i = \ln\left[\frac{p_i(1)}{p_i(0)}\right] = \frac{2y_i}{\sigma^2}$,

where $p_i(1)$ and $p_i(1)$ represents probability of being 1 and 0 for bit i, y_i is the received soft bit values, and σ^2 is the variance of the channel respectively.

2nd Step: Check Node Operation: The expression for check node to bit node messages, R_{ji}, is calculated according to (1)

$$R_{ji} = \left(\prod_{i \in V_{j'}} \alpha_{i'j}\right) \cdot \phi\left(\sum_{i \in V_{j'}} \phi(\beta_{ij})\right) \qquad (1)$$

where

$$\alpha_{ij} = sign(Q_{ij}) \quad \beta_{ij} = |Q_{ij}| \quad \phi(x) = \log\frac{e^x + 1}{e^x - 1}$$

3rd Step: Bit Node Operation : Bit node to check node messages are estimated based on (2).

$$Q_{ij} = \ln\left[\frac{p_i(1)}{p_i(0)}\right] + \left(\sum_{j' \in \mu_{i/j}} R_{j'i}\right) - R_{ji} \tag{2}$$

In this step, the soft decision values, Q_i s, are also estimated from (3), which are then used in (4).

$$Q_i = \ln\left[\frac{p_i(1)}{p_i(0)}\right] + \left(\sum_{j \in \mu_i} R_{ji}\right) \tag{3}$$

4th Step: Syndrome Check: The parity check operations, $\hat{c}H^T$, is performed based on the hard decision variables, $\hat{c}_i$, from equation (4).

$$\hat{c}_i = \begin{cases} 1 & if \quad Q_i < 0 \\ 0 & otherwise \end{cases} \tag{4}$$

If $\hat{c}H^T = 0$ or the number of iterations equals the maximum limit then the decoder is stopped else the decoder goes back to 2nd step and continues iterating.

Offset Min-Sum Algorithm

The SPA is the best performing, yet the most complex algorithm for the decoding of LDPC codes. In the last decade, various complexity reduction schemes for decoding of LDPC codes have been studied. One promising reduced complexity decoding scheme is the Min-Sum algorithm [25][26], which do not require any channel state information and involve only addition and compare operations. In order to improve the accuracy of the check node operation in the Min-Sum algorithm, the output reliability values can be reduced by a positive constant η. This approach is called Offset Min-Sum (OMS) algorithm and can be simply implemented by replacing Equation (1) of SPA with (5).

$$|y_{ji}|_{\min} = \max\left\{\left(\min_{i \in V_{j\setminus i}}\{|Q_{i'j}|\} - \eta\right),\ 0\right\}$$

$$R_{ji} = \left(\prod_{i \in V_{j\setminus i}} \alpha_{i'j}\right) \cdot |y_{ji}|_{\min} \tag{5}$$

Layered Decoding Algorithm

Another promising variation to SPA can be obtained by using a modified message processing schedule, called layered decoding [27]. In this approach, an LDPC code is viewed as a code concatenated from m constituent codes or layers. Consequently, single LDPC decoder iteration consists of m successive sub-iterations performed by each constituent code, and updated messages from previous constituent code are passed to the next constituent codes to be processed in the next sub-iteration. As opposed to the

standard SPA, this technique allows utilization of the updated messages more quickly in the algorithm and leads to faster convergence speeds in the LDPC decoder. Furthermore, processing messages in layers reduces the memory requirement per decoding iteration.

Figure 12 shows a two layer parity check matrix for a (12, 4) LDPC code. Rows of the parity check matrix are grouped into non-overlapping subsets such that each column of this subset has at most a weight of one.

$$H=\left[\begin{array}{cccccccccccc} 1&0&0&0&0&0&0&1&0&1&0&0\\ 0&1&0&0&1&0&0&0&0&0&1&0\\ 0&0&1&0&0&1&0&0&0&0&0&1\\ 0&0&0&1&0&0&1&0&1&0&0&0\\ \hline 0&0&1&0&0&0&0&0&1&0&0&0\\ 0&0&0&1&0&0&0&0&0&1&0&0\\ 1&0&0&0&0&0&0&0&0&0&1&0\\ 0&1&0&0&0&0&0&0&0&0&0&1 \end{array}\right]$$

Figure 12, Layered parity check matrix for a (12, 4) LDPC code

The layered decoding algorithm can be independently applied to SPA or OMS. Layered sum-product algorithm (LSPA) is a simple variation of (1)-(3) and given in (6)-(8). In this case, first all Q_i is initialized to $\frac{2y_i}{\sigma^2}$. Then, for all i (bit node) in the layer k of the rows, (6)-(8) is repeated for one layer after another.

$$Q_{ij} = Q_j - R_{ji} \tag{6}$$

$$R_{ji} = \left(\prod_{i' \in i \setminus N} \alpha_{i'j}\right) \cdot \phi\left(\sum_{i' \in i \setminus N} \phi\left(\beta_{ij}\right)\right) \tag{7}$$

$$Q_j = Q_{ij} + R_{ji} \tag{8}$$

In the case of layered offset min-sum (LOMS) algorithm, equation (7) is replaced by (5).

Simulation Results

In the following, BER comparisons of SPA, OMS, and LOMS Decoding algorithms are provided for a (1728, 864) LDPC code [27]. In the simulations, AWGN channel with zero mean and variance $N_0/2$ is assumed and BPSK modulation is employed. Simulations are carried out until 100 word errors are collected for each SNR point.

In Figure 14, floating point BER performance of the sum-product algorithm and OMS algorithm with various iterations are illustrated. As observed, increasing the number of maximum decoding iterations of SPA from 8 to 16 provides around 1 dB performance improvement while only 0.25 dB improvement is gained by doubling the decoding iterations from 16 to 32. In comparison of OMS to SPA, although reduced complexity OMS decoding algorithm introduces slight performance loss at low SNR values, it performs 0.1 db better compared to SPA at BER of 10^{-6}.

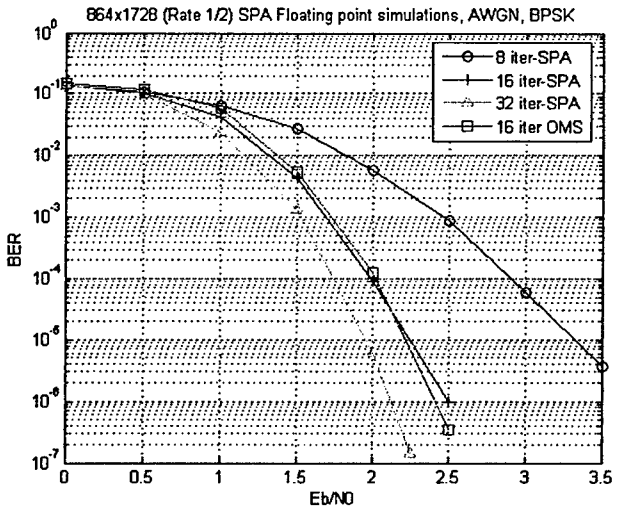

Figure 13, BER performance of (1728,864) LDPC code using SPA and OMS algorithms

Figure 14, compares BER performance of SPA with 16 iterations to Layered OMS algorithm with 8 and 16 iterations. As seen, LOMS algorithm achieves approximately the same error rate performance of SPA with only half of the number of decoding iterations.

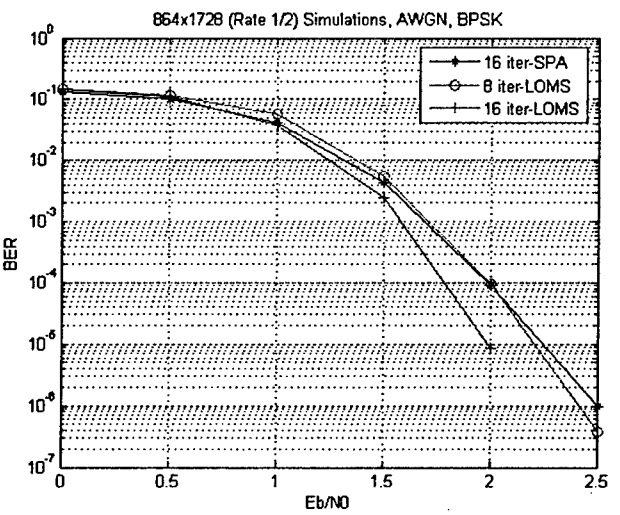

Figure 14, BER and WER performance comparison

A question that remains to be answered is: Is the benefit of LDPC worth the extra complexity as compared to convolution code? To answer this question, we need to design and architect a real-time implementation of LDPC code and compare the performance and complexity with the convolution code. We will leave this task in the Phase II of this effort.

5. Verification with Silvus DSP MIMO Testbed

The designed MIMO-OFDM system has been tested in real channels on an existing Silvus 2x2 MIMO DSP testbed. **Figure 15** shows a system block diagram of the testbed. The testbed operates in the 915MHz ISM band with 26 MHz bandwidth. The analog part is implemented using COTS integrated radios. Communications algorithms could be implemented on the TI6416 DSP or on the host. The entire testbed is hosted in two compact PCI (cPCI) chassis. For the test that has been conducted for this project, the same Matlab simulation code is reused to generate and decode packets. The DSP is responsible for sending the generated packet to the DACs and acquiring data from the ADCs into the on board memory. The packet decoding is done in a non real-time fashion. However, the signal goes through actual channels and RF impairments. A graphical user interface (GUI) was developed to monitor the field test and collect results. **Figure 16** shows a snapshot of the GUI during a test. The GUI provides instant information such as the packet error rate, channel singular values, SNR, etc., as soon as the received packet is decoded. It also enables users to observe the constellation, signal waveforms, and other intermediate receiver results. The designed MIMO-OFDM system has been demonstrated working on this testbed. Both throughput increase by using spatial multiplexing and diversity gain by using STBC were successfully demonstrated. For instance, it is clearly shown in the screenshot that by using STBC, much more reliable communications were achieved for 16QAM. In fact, in that particular test, there was no error for STBC coded 16QAM and less errors for spatial multiplexed 16QAM. The SNR is around 18dB.

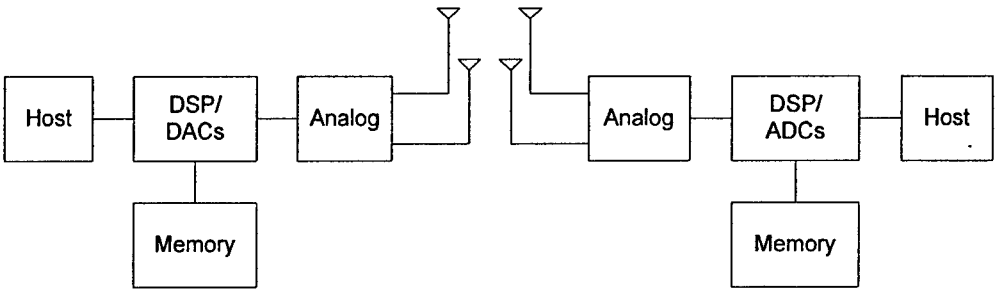

Figure 15. System Block Diagram of Silvus DSP Testbed

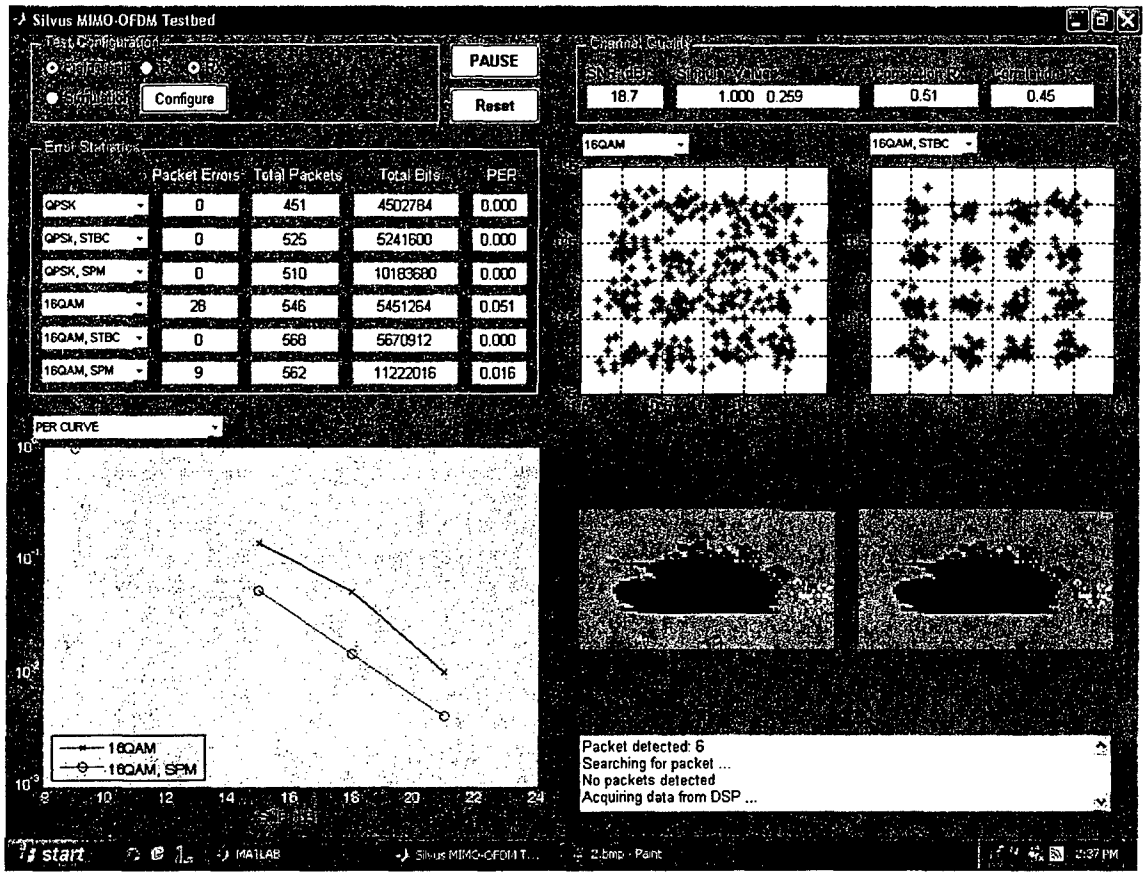

Figure 16. A Screenshot of the Field Test GUI

6. Design and Simulation for High Mobility Extension

To be able to track the highly dynamic changing channel environment like the one experienced by UAV is a complicated one. Due to frequency selectivity in frequency domain and high mobility of mobile reception in high Doppler communication environment, the channel suffers from both frequency and time dispersion. As a consequence of the rapidly time-varying channel, more pilot symbol (PS) are expected in time domain. It is necessary to sample the two-dimensional space (i.e. Frequency and Time) at greater than Nyquist rate of the channel process. To perform the channel estimation/tracking in a high mobile environment, a new data-field structure which is known as 2D checker board pattern pilot symbol assisted modulation (PSAM) is designed and shown in **Figure 16.**

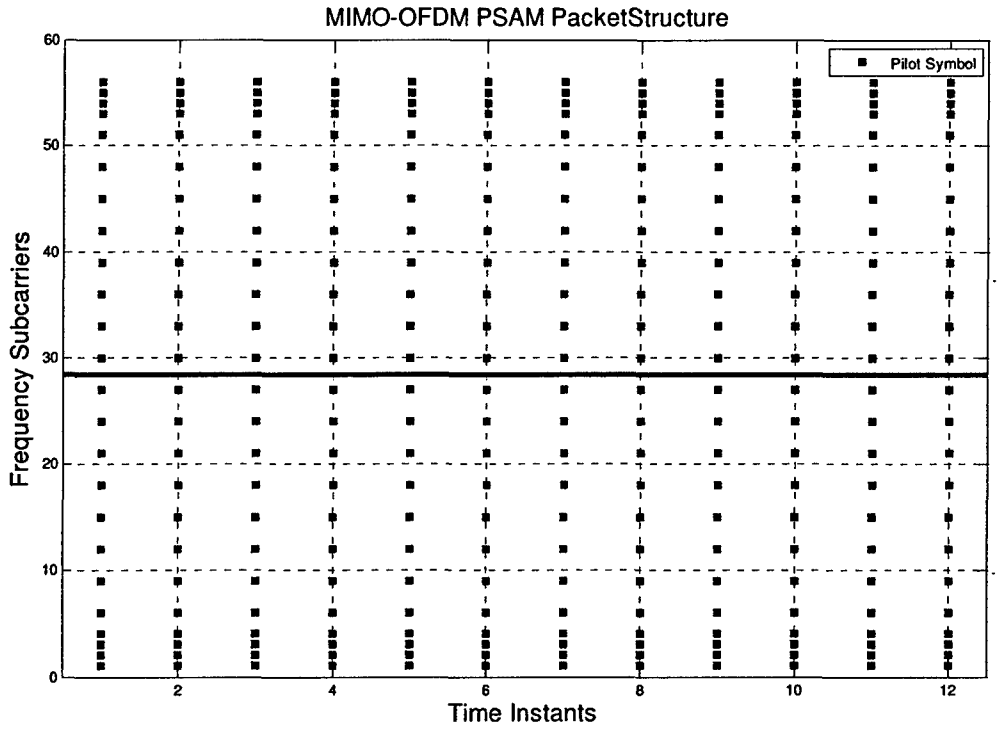

Figure 16, Data-Field PSAM Packet Structure

In practice, known symbols (Pilot Symbols, PS) are inserted at transmitter and channel estimate is acquired by interpolation. The channel estimator consists of linear combinations of the observations at the PS locations. The simplest and highest performing way to process and estimate channel information from MIMO environment is to use orthogonal modulation on each of the transmit antennas. Denote $\mathbf{x}_p$ be observation of pilot value at the receiver and $\mathbf{c}$ be position of data symbols (DS). Due to orthogonality, channel estimates could be obtained by:

$$\hat{\mathbf{c}} = E\left[\mathbf{c}\mathbf{x}_p^{\ H}\right] Cov\left(\mathbf{x}_p\right)^{-1} \mathbf{x}_p \equiv \mathbf{W}\mathbf{x}_p$$

Where $Cov(\mathbf{x}_p)$ is the covariance matrix of PS and **W** is the Wiener Filter coefficients. The current implementation of MIMO-OFDM PSAM Packet channel estimator in Silvus software simulator has a particular OFDM packet structure which contains 12 OFDM symbols, as shown in **Figure 16**. This particular PS placement in the frequency-time grid enables the system to track a frequency roll across the frame. In some situation, the optimum interpolation filter from this sampling of the noisy channel response is a linear filter whose tap coefficients are a function of particular channel statistics. Therefore, the Wiener filter coefficients are often pre-computed and results in an open loop estimation structure which has no acquisition time. Performance of this particular MIMO-OFDM PSAM channel estimation scheme is simulated and the results are presented below.

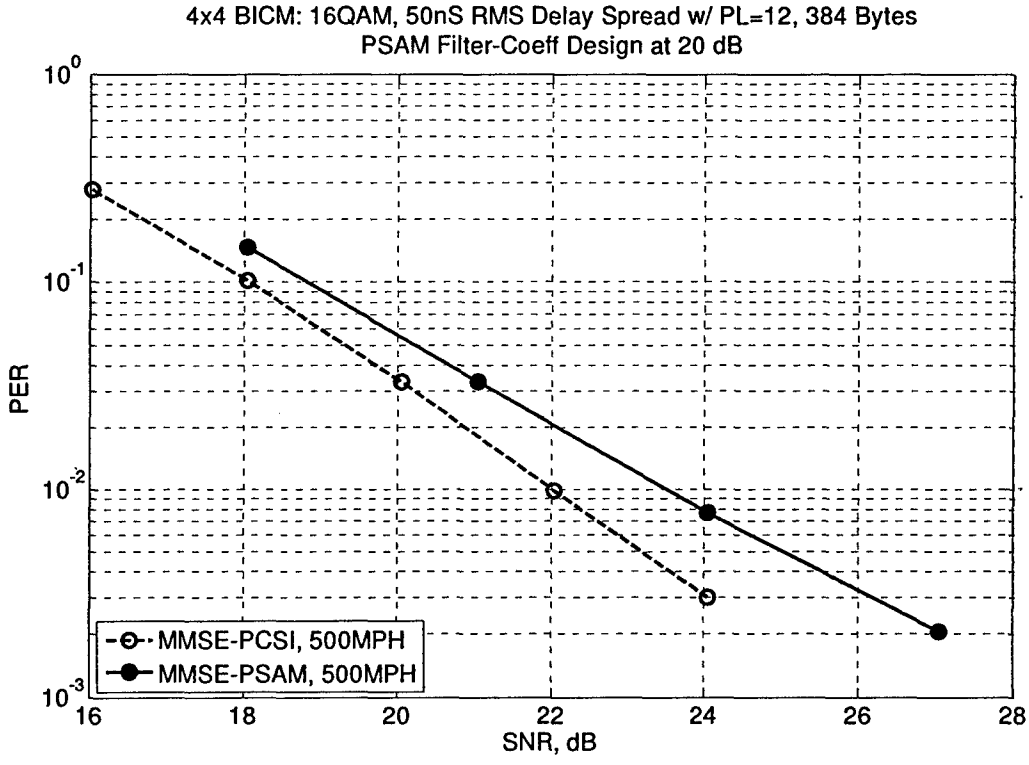

Figure 17, Packet Error Rate for 16QAM Rate-1/2 BICM at 500MPH, Channel D

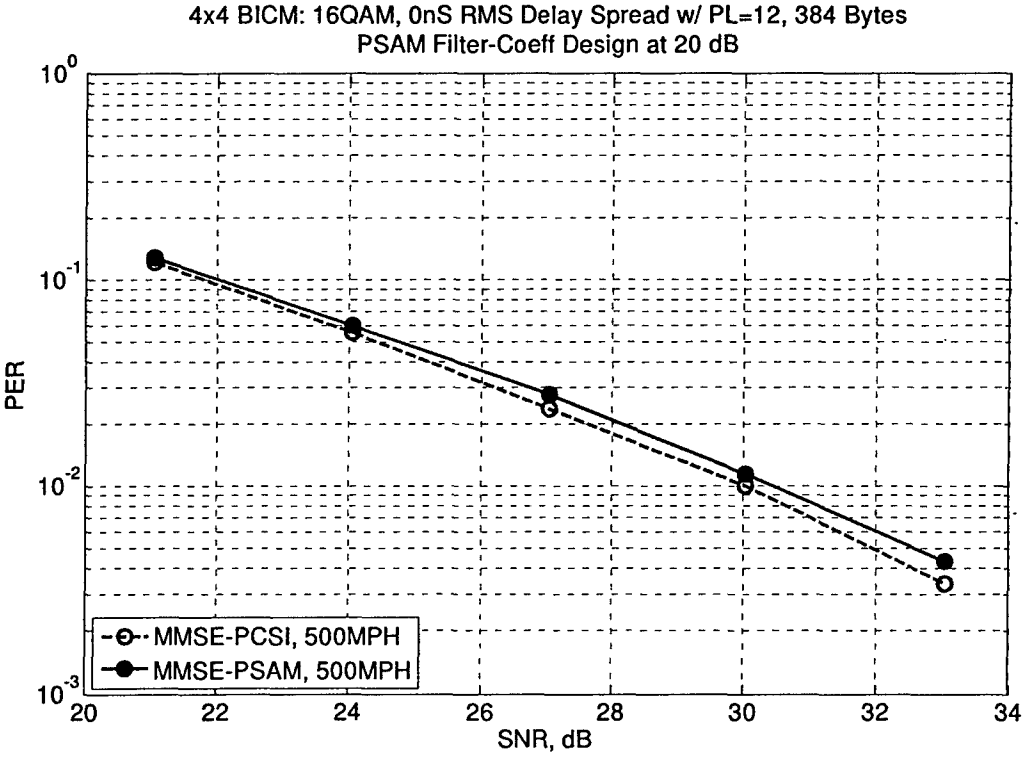

Figure 18, Packet Error Rate for 16QAM Rate-1/2 BICM at 500MPH, Channel A

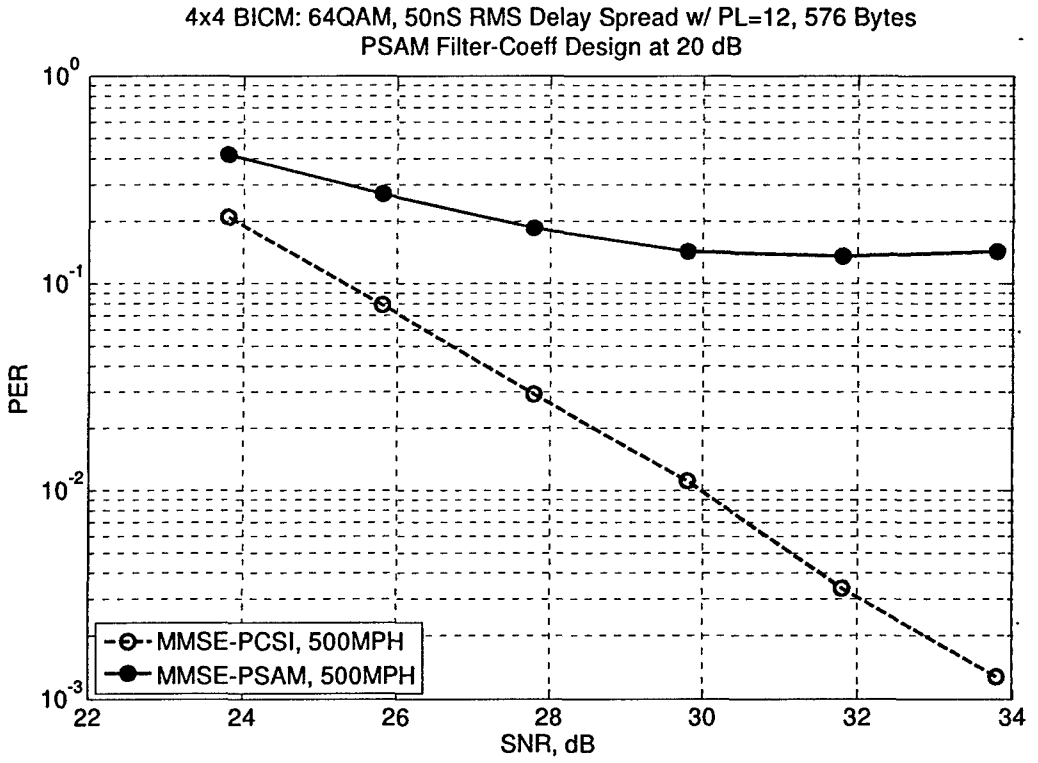

Figure 19, Packet Error Rate for 64QAM Rate-1/2 BICM at 500MPH, Channel D

In our simulations, we assume an equal number of transmit and receive antennas (i.e. 4 x 4 system with 4 spatial streams). Most of OFDM-PHY parameters are compatible with the on-going IEEE 802.11n Next Generation WLAN proposal EWC PHY spec, v1.13. In particular, we assume the following:

- 20MHz bandwidth
- 2.4GHz carrier frequency
- Sub-carrier spacing 312.5KHz
- Bit interleaved coded modulation (BICM) with binary convolution code (BCC) and QPSK, 16QAM and 64QAM
- Time Varying (TV) Jakes model is used for simulation both frequency-flat (FF) or frequency-selective (FS) fading
- Terminal mobility of 500MPH (i.e. 0.72% Normalized Doppler)
- Pre-Computed Wiener Filter Coefficient designed at 20dB SNR and 0.72% Normalized Doppler

We compute the packet error rate (PER). Each packet consists of 1536 symbols. Depending of modulation and coding schemes (MCS), flexible number of information bytes can be sent. We further assume perfect timing synchronization and no frequency offset.

Figure 17 presents a PER performance comparison between perfect channel state information (PCSI) and PSAM of 16QAM Rate-1/2 BICM under Channel-D which is a Non-Light of Sight FS channel with 500MPH. At 1% PER, we observe that PSAM is only ~1.5dB away from PCSI. With the proposed packet structure, we are able to re-construct the channel state information at receiver side fairly accurate even under a high terminal speed of 500MPH.

Figure 18 presents a PER performance comparison between PCSI and PSAM of 16QAM Rate-1/2 BICM under Channel-A which is a FF channel also with 500MPH. In this case, PSAM has performance very close to PCSI with degradation no more than 0.2dB. This is due to the fact that the channel is frequency flat and only varying in time because of high Doppler, so it transforms the original 2D frequency-time interpolation into a single dimension (i.e. time) interpolation. It is quite obvious that with much more resolution in time and PSAM performance gets better.

Figure 19 presents a PER performance comparison between PCSI and PSAM of 64QAM Rate-1/2 BICM under Channel-D which is a Non-Light of Sight FS channel with 500MPH. In this case, we observe that PSAM has an error-floor at about 10% PER. The reason for the error floor is two fold. In general, higher constellation requires not only higher SNR but also more sensitive to channel estimation errors. This is because a denser grid on the constellation plane reduces the pair-wise Euclidean distance. On the other hand, the current packet design assumes a pilot-tone placement of 4 x 4 space-time block of Wash-Hadamard orthogonal sequence. At 500MPH terminal mobility which corresponds to normalized Doppler of 0.72%, the orthogonality assumption is broken and results in an error floor. To further improve the performance of 64QAM, one would need to use a different pilot symbol pattern.

Our preliminary results show that reliable communication with 4x4 16QAM in high mobility could be achieved with time-frequency domain channel tracking. The problem is more challenging with 64QAM. We leave this problem in the Phase II effort when we would optimize the pilot symbol values and placement.

7. Preparation for Real-time Implementation on FPGA

The Silvus-UCLA also investigated on a possible real-time implementation. A real-time implementation offers the following benefits:

- It is closest to an actually deployed system and predicts the achievable performance more accurately.
- It enables more extensive field test.
- It enables field test in a networked environment.
- It enables field test of certain PHY algorithm such as feedback MIMO, which is otherwise impossible or not accurate. Feedback MIMO could significantly improve the system capacity and anti-jam performance.

Two important tasks have been finished: identifying the development platform and mapping key floating point algorithms to fixed-point algorithms.

- Silvus team conducted extensive search for available COTS FPGA development platform and have identified a set of FPGA boards from Nallatech (www.nallatech.com) that offers enough processing power for an advanced 4x4 MIMO communication system with 40MHz bandwidth. The identified FPGA development platform is in compact PCI form factor and supports a scalable architecture. Up to 4 high performances Xilinx FPGA and 8 DACs and ADCs can be supported on a single cPCI board. This platform provides enough processing performance as well as a simple analog baseband I/Q interface. A complete 4x4 MIMO communication system could be easily put together by using using a COTS RF product such as MAX2829.

- Fixed point architecture of major receiver blocks has been defined. Fixed point algorithm has been designed and implemented for most receiver algorithms that involve floating point

arithmetic operations. The most critical part of the receiver is perhaps the MIMO detection. Here we present simulation results of our fixed point MMSE MIMO detection.

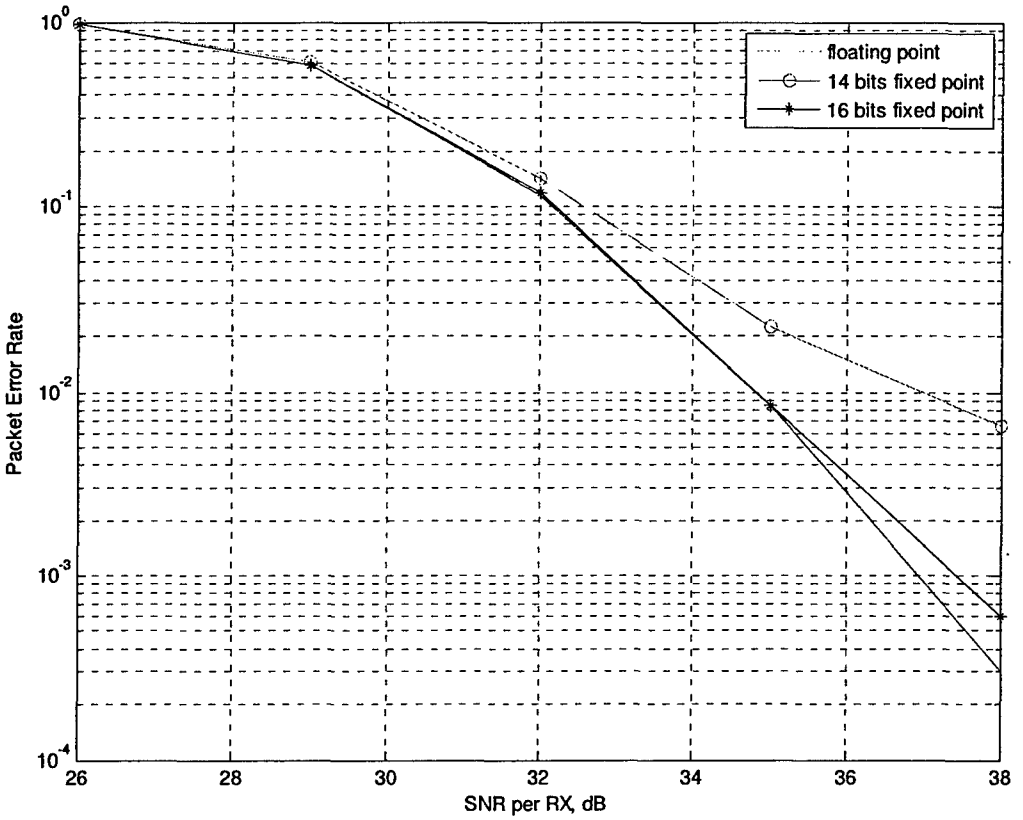

Figure 17. Performance of Fixed Point MMSE MIMO Detection

Our fixed point MMSE MIMO detection is implemented based on QR decomposition followed by a set of matrix vector multiplications. Figure 17 shows the performance of the fixed point implementation in a 4x4 64QAM system with rate 2/3 convolution code. This system achieves an information bit rate of 192Mbps over a 20 MHz bandwidth and puts very strong requirement on the accuracy of the MIMO detection. The number of bits indicated in the plot is the number of bits used during the QR decomposition process. The matrix vector multiplication can be implemented at a less number of bits without noticeable performance loss. With 16 bit implementation, the performance is almost identical with floating implementation for PER above 1% and suffers only 0.5 dB loss at 0.1% PER. The 14 bit implementation lose more at high PER but is a good choice if PER requirement is low.

8. Conclusion

During the Phase I period of this contract, we have successfully designed a MIMO-OFDM packet structure that supports non-line-of-sight communication in an urban warfare. The packet structure

supports a variety of features that are configurable on a packet by packet basis. Those configurable features offer the possibility of optimum bandwidth efficiency, reliability, and complexity tradeoff in a diverse warfare environment. A complete end-to-end physical layer simulation platform has been constructed in Matlab. The feasibility of the developed packet structure and receiver algorithm has been verified on the Silvus DSP MIMO Testbed. We have also finished fixed point implementation for all the key modules of the receiver and identified a cPCI based FPGA platform for real-time implementation.

The work that has been completed in this period laid a solid foundation for Phase II. In other words, we are fully prepared to implement on a FPGA platform a real-time MIMO packet communication system that meets the need of non-line-of-sight urban warfare communications.

References

[1] S. M. Alamouti, "A simple transmit diversity technique for wireless communications", IEEE JSAC, vol 16, Oct. 1998.

[2] V. Tarokh, N. Seshadri, A. R. Calderbank, "Space-time codes for high data rate wireless communication: Performance criteria and code construction", IEEE Trans. Info Theory, vol 44, pp744-765, Mar 1998.

[3] S. Lang, R. Rao, B. Daneshrad, "Design and Development of a 5.25GHz Software Defined Wireless OFDM Communication Platform", IEEE Communications Magazine, Radio Communications Supplement, June 2004.

[4] J. Frigon, B. Daneshrad, "Field measurements of high speed QAM wireless transmission using equalization and real-time beamforming," GLOBECOM'99.

[5] J. Frigon, B. Daneshrad, J. Putnam, E. Berg, Ryan Kim, T. Sun, H. Samueli, "Field trial results for high-speed wireless indoor data communications," IEEE JSAC, vol.18, no.3, March 2000.

[6] G. Foschini, and M. Gans, "On Limits of Wireless Communications in a Fading Environment when Using Multiple Antennas," Wireless Personal Communications, vol. 6, no.3, pp. 311-335, March 1998.

[7] G. Foschini, "Layered Space-Time Architecture for Wireless Communication in a Fading Environment when Using Multi-Element Antennas," Bell Labs Technical Journal, vol. 1, no. 2, pp. 41-59, Fall 1996.

[8] Weijun Zhu, Daniel Liu, David Browne and Michael P. Fitz, "Experiments in Space-Time Modulation," Asilomar Conference on Signals, Systems, and Computers, Nov. 2004.

[9] Raghu Mysore Rao, Weijun Zhu, Stephan Lang, Christian Oberli, David Browne, Jatin Bhatia, Jean-François Frigon, Jingming Wang, Parul Gupta, Heechoon Lee, Daniel N. Liu, ShingWa G. Wong, Mike Fitz, Babak Daneshrad, and Oscar Takeshita. "Multi-Antenna Testbeds for Research and Education in Wireless Communications," IEEE Communications Magazine, Dec. 2004.

[10] J. C. Guey, M. P. Fitz, M. R. Bell, and W.Y. Kuo. Signal design for transmitter diversity wireless communication systems over Rayleigh fading channels. In *Proc. of IEEE Vehicular Technology Conference*, volume 1, pages 136-140. Atlanta, GA, 1997.

[11] Teletar, "Capacity of Multi-antenna Gaussian Channels," European Transactions on Telecomm. Vol. 10, pp. 585-595, 1999.

[12] Pattanavichate J, Sieskul BT, Jitapunkul S. "Capacity assessment of MIMO channel model accounted for Rayleigh fading and local scattering," *2004 International Symposium on Intelligent Signal Processing And Communication Systems ISPACS 2004 pp.531-5.*

[13] Ting S, Sakaguchi K, Araki K., "Performance analysis of MIMO eigenmode transmission system under realistic channel and system conditions," *IEICE Transactions on Communications, vol.E87-B, no.8, Aug. 2004, pp.2222-32.*

[14] Rao RM, Lang S, Daneshrad B. "Indoor field measurements with a configurable multi-antenna testbed," *GLOBECOM '04, pp.3952-6*

[15] M. Fitz, J. Grimm, S. Siwamogsatham, "A new view of perfomance analysis techniques in correlated Rayleigh fading, Proc. IEEE WCNC, 1999, pp. 139-144.

[16] Chen T-A, Fitz MP, Shengchao Li, Zoltowski MD. "Two-dimensional space-time pilot-symbol assisted demodulation for frequency-nonselective Rayleigh fading channels," *IEEE Transactions on Communications, vol.52, no.6, June 2004, pp.953-63.*

[17] Rao RM, Daneshrad B. "I/Q mismatch cancellation for MIMO-OFDM systems," *2004 IEEE 15th International Symposium on Personal, Indoor and Mobile Radio Communications, Vol.4, 2004, pp.2710-14 Vol.4.*

[18] Oberli C, Daneshrad "B. Maximum likelihood tracking algorithms for MIMO-OFDM," *2004 IEEE International Conference on Communications Vol.4, 2004, pp.2468-72.*

[19] Syed Aon Mujtaba, John Sadowsky, and Jeff Gilbert, "Single-Pole Single-Zero Model for Phase Noise in OFDM Systems," IEEE 802.11-04/0177-00-000n.

[20] Mark Webster, "Suggested PA model for 802.11 HRb," IEEE 802.11-00/294.

[21] W.C. Jakes, "*Microwave Mobile Communications*", Piscataway, NJ: IEEE Press, 1994.

[22] A.A.M Saleh and R.A. Valenzuela, "A statistical model for indoor *multi*path propagation," *IEEE Joumal* on *Selected Areas in Communicotions,* vol. SAC-5, no.2, pp. 128-137. February 1987.

[23] R. G. Gallager, Low-density parity-check codes," *Cambridge, MA: MIT Press*, 1963.

[24] D. J. C. MacKay, "Good error-correcting codes based on very sparse matrices," *IEEE Trans. Inf. Theory*, vol.45, no.2, pp.399–431, Mar.1999.

[25] M. Fossorier, M. Mihaljevic and H. Imai, "Reduced Complexity Iterative Decoding of Low-Density Parity Check Codes Based on Belief Propagation", *IEEE Transactions on Communications*, vol. 47, pp. 673-680, May 1999.

[26] J. Chen and M. Fossorier, "Density evolution for two improved BP-based decoding algorithms of LDPC codes," *IEEE Commun. Letters*, vol. 6, pp. 208–210, May 2002.

[27] "TGn Sync Proposal Technical Specification," available at http://www.tgnsync.org/techdocs/